Contents lists available at AccScience Publishing
Nonlinear Science and Control Engineering (NSCE)
Vol. 2, No. 3 (2026)
https://accscience.com/journal/nsce

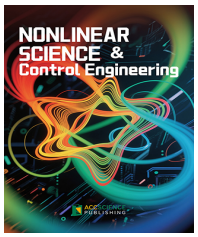

Frequency- and bit-rate-adaptive compression of electromyography signals by wavelet packet transform and optimal scalar quantizer bit rate allocation

Joseph Mvogo Ngono[1], Arnaud Nanfak[2], Jean de Dieu Nkapkop[3]*, Auguste Noumsi Woguia[1], Christophe Lessouga Etoundi[3], Zeric Tabekoueng Njitacke[4], and Pierre Ele[5]

[1]*Applied Computing Laboratory, Faculty of Science, University of Douala, Douala, Littoral Region, Cameroon*
[2]*Laboratory of Electronic, Electrical Engineering, Automation and Telecommunication, National Higher Polytechnic School of Douala, University of Douala, Douala, Littoral Region, Cameroon*
[3]*Technology and Applied Sciences Laboratory, University Institute of Technology, University of Douala, Douala, Littoral Region, Cameroon*
[4]*Department of Electrical and Electronic Engineering, College of Technology, University of Buea, Buea, Littoral Region, Cameroon*
[5]*Laboratory of Electrical Engineering, Mechatronic and Signal Treatment, National Advanced School of Engineering, University of Yaoundé 1, Yaoundé, Centre Region, Cameroon*

Article History:
Received: March 30, 2026
Revised: April 28, 2026
Accepted: May 18, 2026
Published online: June 23, 2026

A B S T R A C T
Electromyography (EMG) signals are widely used for neuromuscular assessment, rehabilitation, and prosthetic control, but their high sampling rates and long recording durations generate large data volumes. This study presents a frequency- and bit-rate-adaptive compression method for EMG signals based on wavelet packet transform and optimal scalar quantizer bit allocation. The method first decomposed the signal using a complete wavelet packet tree of depth L = 5. Then, the coefficients of each sub-band were modeled as generalized Gaussian distributions, and analytical rate-distortion estimates were derived for a uniform scalar quantizer. These estimates were used in a Lagrangian optimization framework to jointly select the optimal wavelet packet basis and allocate quantization bit rates to achieve the target compression ratio. Experiments were conducted on four EMG records, including two surface EMG signals and two needle EMG signals, using Daubechies db2 and biorthogonal bior4.4 wavelets over compression ratios from 5 to 25. The proposed method was compared with a conventional wavelet-based baseline using root-mean-square error (RMSE), signal-to-noise ratio (SNR), percentage root-mean-square difference (PRD), and quality score (QS). Across all tested operating points, the optimal adaptive configuration reduced RMSE and PRD by 37.7% on average, increased SNR by 4.33 dB, and improved QS by 69.5% compared with the optimal baseline configuration. These results highlight the effectiveness of the proposed adaptive framework, making it well-suited for real-time biomedical signal compression and telemedicine applications.

Keywords: Frequency- and bit-rate-adaptive compression; Electromyography signal; Wavelet packet transform; Scalar quantizer bit rates

***Corresponding author**:
Jean de Dieu Nkapkop (jdd.nkapkop@ltsa-univ-dla.com).

Citation:
Ngono JM, Nanfak A, de Dieu Nkapkop J, *et al*. Frequency- and bit-rate-adaptive compression of electromyography signals by wavelet packet transform and optimal scalar quantizer bit rate allocation. *Nonlinear Sci Cont Eng.* 2026;2(3):026140011. doi: 10.36922/NSCE026140011

Copyright: © 2026 The Author(s). This is an Open Access article distributed under the terms of the Creative Commons Attribution License, permitting distribution, and reproduction in any medium, provided the original work is properly cited.

1. Introduction

Electromyography (EMG) signals are electrical signals generated by muscle activity. These signals are commonly used in medical and research settings to analyze muscle function and diagnose neuromuscular disorders. EMG signals are often sampled at high rates, producing large amounts of data that require efficient compression techniques to store and transmit effectively.

Various key EMG compression techniques exist; lossless compression techniques[1–3] allow for the exact reconstruction of the original EMG signal from the compressed data. These techniques are essential when it is critical to maintain the integrity of the original signal. On the other hand, lossy compression techniques[4–7] reduce data size by approximating the original signal, potentially resulting in some information loss. These techniques are often used when a slight loss of signal fidelity is acceptable. In this second category, transform-based methods[8–10] (e.g., wavelet transform) and model-based methods[11–13] (e.g., neural network-based approach) are currently used for lossy EMG compression. Related work on other biomedical signals includes wavelet packet compression for electrocardiography (ECG)[14,15] and deep learning-based compressed sensing for electroencephalography (EEG).[16,17]

While both wavelet transform compression schemes and model-based coding offer powerful tools for EMG signal compression, they have inherent limitations that must be addressed. The wavelet transform faces several challenges when applied to rapidly varying EMG signals; non-stationarity and frequency leakage are key limitations.[18] A comprehensive review of wavelet applications in EMG analysis by Phinyomark *et al*.[19] clarifies these challenges. Addressing these issues may involve using adaptive wavelet techniques to optimize the wavelet basis for specific signal characteristics. Similarly, the model-based assumptions and sensitivity to noise in those models can limit their effectiveness for the non-linear and noisy nature of EMG signals.[20] Overcoming these limitations may require adaptive techniques for selecting the best basis in the rate-distortion sense and for optimal bit allocation in the quantization stage.[21,22] However, the optimization process that minimizes distortion for a specified bit rate or reduces the bit rate for a given level of distortion involves evaluating multiple bases and selecting the one that provides the optimal balance between compression efficiency and signal quality, which can be computationally intensive.[23,24]

Recent advances in biomedical signal compression have explored diverse directions. Subasi *et al*.[25] leveraged wavelet packet decomposition for EEG-based biometric authentication, demonstrating its continued relevance for non-stationary neural signals. Erkoc[26] proposed a deep learning-based compressed sensing method for ECG signals, achieving high signal-to-noise ratios (SNRs) at low sensing rates using unrolled architectures; however, deep learning approaches require large training datasets and significant computational resources. A comprehensive 2026 review on EMG signal processing[27] highlights that non-stationarity, inter-session variability, and electrode displacement remain open challenges, and that many deep learning solutions struggle with real-time deployment on embedded systems. These recent works confirm that there is still a need for lightweight, analytical compression methods that do not rely on training data, can adapt to signal non-stationarities, and provide closed-form rate-distortion guarantees. Transformer architectures for biosignal analysis were reviewed by Anwar *et al*.,[28] while recent methodological advances in EMG gesture recognition were surveyed by Shin *et al*.[29]

To address this gap, we proposed a novel frequency-adaptive compression scheme that adapts the compression process to the different frequency bands of the signal. In contrast to the computationally time-consuming operational rate-distortion approach proposed for best-basis selection,[30,31] our method reduces complexity by providing closed-form expressions of the rate-distortion function. This is achieved by assuming a generalized Gaussian distribution (GGD) for wavelet packet sub-band coefficients and using a uniform scalar quantizer. The main contributions can be summarized as follows:

- We introduce a novel frequency- and bit-rate-adaptive compression scheme that adapts the compression process to the different frequency bands of the signal and different bit-rate targets.
- We combine rate-distortion curve estimation and a Lagrangian optimization technique on a tree-structured wavelet packet-admissible basis to derive both the best basis and the optimal quantizer parameters for each sub-band.

The structure of this paper is as follows: an introduction (Section 1) that emphasizes the importance of EMG signals in medical and technological applications, reviews existing compression techniques (both lossless and lossy) and their limitations, and introduces the proposed frequency- and bit-rate-adaptive compression scheme along with its advantages. The methods section (Section 2) elaborates on the use of wavelet packet transform for non-stationary EMG signals, the selection of optimal wavelet packet bases using an additive cost function, and the allocation of scalar quantizer bit rates via rate-distortion analysis. It also describes the GGD for modeling sub-band coefficients and explains the algorithm for adaptive compression, including steps such as wavelet packet transform computation, rate-distortion curve approximation, and best basis selection. The metrics used, such as SNR, percentage root-mean-square difference (PRD), compression ratio (CR), and quality score (QS), are also described. In Section 3, quantitative results are presented, showcasing the method's superior compression efficiency and signal quality, and highlighting the method's effectiveness in optimizing compression while preserving signal fidelity. Finally, the Conclusion (Section 4) summarizes the key contributions and performance of the proposed scheme, emphasizing its potential for application in biomedical signal processing and real-time medical systems.

2. Methods

Wavelet decomposition concentrates signal energy at low frequencies for EMG signals that exhibit local regularity, particularly those admitting a good local polynomial approximation. When there are areas of rapid local variation and non-stationarities, the wavelet transform is suboptimal. To describe this particular class of EMG signals, a wide family of basic functions, called wavelet packets, was used in the frequency adaptive compression chain.

This algorithm has three main parts: (i) wavelet packet decomposition, (ii) selection of the best basis, and (iii) op-

timal allocation of scalar quantizer bit rates based on rate-distortion curve estimation and entropy coding. Each part is succinctly described in the subsections that follow.

2.1. Wavelet packet transform

The wavelet packet transform is based on the mother wavelet ψ(t) and the scaling function ϕ(t), defined by **Equations 1 and 2**, respectively.

$$\phi(t) = \sum_k h_k \phi(2t - k) \tag{1}$$

$$\psi(t) = \sum_k g_k \phi(2t - k) \tag{2}$$

The overall compression chain, including wavelet packet decomposition, best basis selection, optimal scalar quantization, and entropy coding, is illustrated in **Figure 1**.

The wavelet packet transform is a generalization of the classical wavelet transform.[30,31] Wavelet packet-based analysis has been widely applied to biomedical signals for efficient representation and time–frequency analysis.[32] Wavelet packets are a collection of orthogonal bases that are better adapted to the non-stationarities of EMG signals. This family has, among others, the wavelet bases, the Walsh functions, and the regular Walsh functions. This basic collection is organized as a one-dimensional signal following a complete binary tree structure.

The complete collection of bases is obtained by recursively decomposing the low- and high-frequency sub-bands to a given depth L of the tree. Each eligible base appears as a subtree obtained through a tree path from the root node. **Figure 2** shows the binary tree structure of wavelet packet decomposition up to depth L.

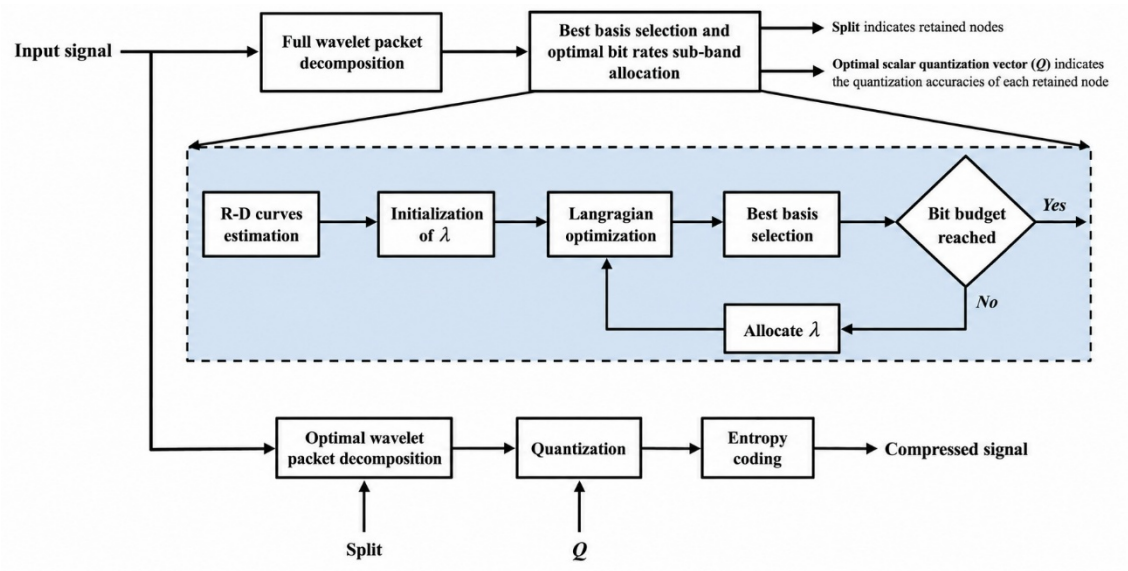

Figure 1. Overall compression chain for electromyography signals based on the wavelet packet transform, including best basis selection, optimal scalar quantization, and entropy coding.

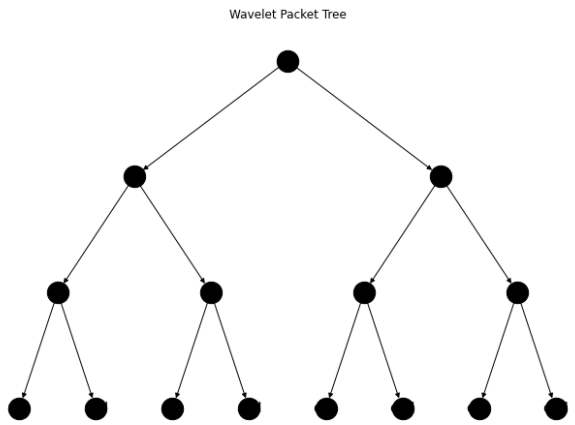

Figure 2. Binary tree structure of wavelet packet decomposition up to depth L = 5, showing the recursive splitting of both approximation and detail sub-bands.

For a given signal *s*(*t*), the wavelet packet decomposition at level *j* can be written as:

- Approximation coefficients:

$$a_{j+1}[n] = \sum_k h_k a_j[2n - k] \tag{3}$$

- Detail coefficients:

$$d_{j+1}[n] = \sum_k g_k a_j[2n - k] \tag{4}$$

The recursive decomposition can be applied to both the approximation and detail coefficients at each level. The equations become more generalized, and the node decompositions are given by **Equations 5 and 6**:

$$w_{2n}[j+1, k] = \sum_m h[m - 2k] w_n[j, m] \tag{5}$$

$$w_{2n+1}[j+1, k] = \sum_m g[m - 2k] w_n[j, m] \tag{6}$$

To reconstruct the signal from the wavelet packet coefficients, we used the inverse process. The reconstruction process can be performed using approximation coefficients and detail coefficients (**Equation 7**) or general coefficients (**Equation 8**).

$$a_j[n] = \sum_k h[k-2n]a_{j+1}[k] + \sum_k g[k-2n]d_{j+1}[k] \quad (7)$$

$$\begin{aligned} w_n[j,m] &= \sum_k h[m-2k]w_{2n}[j+1,k] \\ &+ \sum_k g[m-2k]w_{2n+1}[j+1,k] \end{aligned} \quad (8)$$

The basic functions for the wavelet packet transform can be written as:

$$\begin{aligned} \psi_{j,n}(t) = &\sum_k h[k]\psi_{j+1,2n}(2t-k) + \\ &\sum_k g[k]\psi_{j+1,2n+1}(2t-k) \end{aligned} \quad (9)$$

In this study, the Daubechies db2 wavelet was selected as a reference mother wavelet due to its favorable trade-off between compact support, regularity, and computational efficiency, making it well-suited for capturing the transient and non-stationary characteristics of EMG signals. To further illustrate the flexibility of the proposed approach, a bi-orthogonal wavelet (bior4.4) was also considered in the experimental analysis. It is important to note that the proposed method does not rely on a fixed basis, as the wavelet packet framework enables the adaptive selection of the best basis within a large dictionary of admissible bases derived from the chosen mother wavelet. More generally, the methodology can be extended to other wavelet families, such as Symlets and Coiflets, depending on the signal characteristics and application requirements. Nevertheless, the choice of the mother wavelet may influence the overall performance of the compression scheme.

2.2. Best basis selection and the sub-bands' bit rate allocation

The selection of the best basis relies on an additive cost function *J* that satisfies the condition described in **Equation 10**.

$$J(0) = 0 \; and \; J\left(\sum_i X_i)\right) = \sum_i J(X_i) \quad (10)$$

The criterion used in this work was the Lagrangian's expression:

$$J(\lambda) = D + \lambda R \quad (11)$$

which enables minimizing distortion while respecting a bit-rate constraint.[21] In the Lagrangian's expression, *D* represents the distortion and *R* the bit rate. Lightweight hybrid networks for sparse EMG[33] share similar rate-distortion objectives. The allocation of bit rates and the sub-bands' choice are carried out following the steps described below:

- Step 1: Decompose the EMG signal using all basis collections into wavelet packets, up to depth L of the tree. the coefficients $C^l_{k.}$ are obtained.
- Step 2: For each sub-band corresponding to the node n^l_k, evaluate the rate-distortion function using a GGD model for the sub-band data distribution and estimate the rate-distortion curve. For several quantization accuracies q, we derived the bit rates $R_{q\in Q}\left(n^l_k\right)$ and the associated distortions $D_{q\in Q}\left(n^l_k\right)$.
- Step 3: Initialize the parameter λ for each node of the tree corresponding to the sub-band n^l_k, and determine the minimum of the Lagrangian:

$$J^l_k(\lambda) = \min_{q\epsilon Q}\left[D_q\left(n^l_k\right) + \lambda R_q\left(n^l_k\right)\right] \quad (12)$$

- Step 4: Initialize the current depth l of the tree at L. We made $q^*\left(n^l_k\right) = argmin\left(J^l_k(\lambda)\right)$, which corresponds to the current optimal quantization precision of the band n^l_k for the λ parameter. Initialize:

$$\begin{cases} \widetilde{J^l_k} = J^l_k \\ \widetilde{R^l_k} = R^l_k \\ \widetilde{D^l_k} = D^l_k \\ Split\left(n^l_k\right) = 0 \end{cases} \text{where} \begin{cases} R^l_k = R_{q^*\left(n^l_k\right)} \\ D^l_k = D_{q^*\left(n^l_k\right)} \end{cases} \quad (13)$$

- Step 5: For l equals to $L-1$ to l equals to 0:

$\forall\, k = 1, 2, \ldots..2^l$ at the lth tree level
If $\left(J^l_k(\lambda) < \widetilde{J^{l+1}_{2k-1}(\lambda)} + \widetilde{J^{l+1}_{2k}(\lambda)}\right)$ then
$Split\left(n^l_k\right) = 0$
$\widetilde{R^l_k} = R^l_k$
$\widetilde{D^l_k} = D^l_k$
$\widetilde{J^l_k} = J^l_k$
Else
$Split\left(n^l_k\right) = 1$
$\widetilde{R^l_k} = R^{l+1}_{2k-1} + R^{l+1}_{2k}$
$\widetilde{D^l_k} = D^{l+1}_{2k-1} + D^{l+1}_{2k}$
$\widetilde{J^l_k} = J^{l+1}_{2k-1} + J^{l+1}_{2k}$
End if
End for

- Step 6: Browse the tree from the root n^0_0 and extract the optimal subtree that corresponds to the best wavelet packet base and the optimal quantization precision of the associated sub-band for the λ parameter.
- Step 7: Iterate Steps 3, 4, 5, and 6 for a parameter sequence λ, up to the optimum λ^* to reach the desired bit budget.

The selection of the best basis in the rate-distortion sense involves choosing a wavelet packet basis that minimizes distortion for a given bit rate or minimizes the bit rate for a given level of distortion. This process usually involves evaluating multiple bases and choosing the one that provides the best balance between compression efficiency and signal quality. The complexity of the algorithm for selecting the optimal basis can be divided into several steps:

- Wavelet packet transform computation
- Rate-distortion curves computation
- Best basis selection

The wavelet packet transform computation is classical; instead of calculating the operational rate distortion,[21] which is computationally intensive, we modeled the *j*-th sub-band coefficients of the signal using a GGD and estimated the rate-distortion curve using the method described in Section 2.3.

2.3. Approximations of the rate-distortion curve in each sub-band

Let us assume that the source to be quantized consists of *J* sub-bands, each containing n_j coefficients, where *j* ranges from 1 to *J*, and the total number of coefficients is given by $n = \sum_j n_j$. GGD has been widely used to model the distribution of wavelet coefficients.[34] For wavelet packet coefficients, we modeled the coefficients in each sub-band *j* using a probability density function (**Equation 14**).

$$\begin{aligned} f\left(x;\alpha_j,\beta_j,\mu_j\right) = &\frac{\beta_j}{2\alpha_j\Gamma\left(\frac{1}{\beta_j}\right)} \\ &\exp\left(-\left(\frac{|x-\mu_j|}{\alpha_j}\right)^{\beta_j}\right) \end{aligned} \quad (14)$$

where $\beta_j > 0$ and $\alpha_j > 0$ and Γ is the gamma function. This involves estimating the scale parameter α_j, the shape parameter β_j and the mean parameter μ_j for each sub-band.

At high bit rates, the rate-distortion curve can be approximated using Bennett's high-rate approximation for GGD (**Equation 15**).

$$R_j(D) \approx \frac{1}{2}\log_2\left(\frac{G_{\beta_j}{\alpha_j}^2}{D}\right) \tag{15}$$

where $G_{\beta_j} = \frac{\Gamma\left(\frac{3}{\beta_j}\right)}{\Gamma\left(\frac{1}{\beta_j}\right)}$

Equation 15 is valid at high rates. These approximations are also needed at low bit rates. To overcome this task, we proposed the following method, which is inspired by the approach used in a previous study.[34] However, our method differs in that we directly estimate the rate-distortion curve and the distortion, rather than separately estimating the rate and the distortion.

We assumed that the wavelet packet coefficients were quantized using a uniform scalar quantizer with a quantization step $\Delta_j > 0$ for each sub-band. In uniform scalar quantization, the range of values the source can take is divided into equally spaced intervals, known as quantization levels. The quantizer assigns a representative value, typically the midpoint, to each interval. For a uniform quantizer, the range $[x_{\max}, x_{\min}]$ of the source values is divided into L intervals of equal width. Generally, rate-distortion algorithms based on analytical methods use the standard Bennett formula to approximate the rate-distortion curve; however, in this paper, we opted for the asymptotic formula developed in a previous study.[35]

Let us consider the Bennett's high-rate approximation for GGD given in **Equation 15**. This equation is only applicable at high resolution (i.e., when Δ_j is small). To create an approximation suitable for both high and low resolutions, we replaced the previous approximation with another rate-distortion curve $\boldsymbol{D} = (\boldsymbol{D}_1, \boldsymbol{D}_2, \ldots\ldots, \boldsymbol{D_J})$, as defined in **Equation 16**.

$$\begin{aligned}&\forall j \in \{1, 2, \ldots\ldots J\},\\ &R_j(D_j) = a_j^k D_j + c_j^k \text{ if } D_j^{(rd,k-1)} < D_j < D_j^{(rd,k)}\end{aligned} \tag{16}$$

with k $\in \{1, 2, \ldots\ldots m^{rd}\}$ and the parameter m^{rd} is a given input representing the number of intervals or segments used to approximate the rate-distortion curve. Thus, we suppose that: $D_j^{(rd,0)} \leq D_j^{(rd,1)} \leq D_j^{(rd,2)} \leq \ldots\ldots < D_j^{(rd,m^{rd})}$.

Please note that the superscript (rd) is used to distinguish the intervals of the rate-distortion curve approximation from those of the distortion approximation. To ensure a decreasing function, the coefficients (a_j^k), for $1 \leq k \leq m^{rd}$, must be negative. Additionally, each coefficient (c_j^k) is selected to maintain R_j as a continuous function. Since the rate should be non-negative, we also require that $R_j(D_j)$ equals to 0 for all $D_j \geq D_j^{(rd,m^{rd})}$. This condition enables us to determine $D_j^{(rd,m^{rd})}$ by identifying the first point D_j, where $R_j(D_j)$ equals to 0. For the other points $D_j^{(rd,k)}$, where $1 \leq k \leq m^{rd} - 1$, they are chosen to ensure that the resulting piecewise affine function closely approximates the rate-distortion curve. In the first interval, a well-known close approximation for the rate-distortion at high bit rate is provided by the Bennett formula, leading to:

$$\forall j \in \{1, 2, \ldots\ldots J\}, R_j(D_j) \approx \frac{1}{2}\log_2\left(\frac{G_{\beta_j}{\alpha_j}^2}{D_j}\right) \tag{17}$$

We thus obtained the rate-distortion approximation $R_j(D_j)$ on the first interval.

Then, we derived (a_j^2, c_j^2) such that $R(D_j)$ on the interval $\left[D_j^{(rd,1)}, D_j^{(rd,2)}\right]$ is tangent to the rate-distortion function at an arbitrary point $D_j > D_j^{(rd,1)}$. After that, the value of $D_j^{(rd,1)}$ can be selected by identifying the configuration where the approximation error between the rate-distortion curve and the function $R(D_j)$ on the interval $\left[D_j^{(rd,0)}, D_j^{(rd,2)}\right]$ is small. By following the same strategy, we deduced the remaining values of $D_j^{(rd,2)}$, $D_j^{(rd,3)}, \ldots\ldots D_j^{(rd,m^{rd}-1)}$.

Let us now consider the distortion approximation with respect to the quantization step Δ_j. We also used the following piecewise exponential approximation of the distortion (for an order moment $p_j > 1$; **Equation 18**).

$$\begin{aligned}&\forall j \in \{1, 2, \ldots\ldots J\},\\ &l_j = \log_2(\Delta_j)\, d_j(l_j) = \frac{\eta_j(p_j+1)}{\nu_j}\left(d_j^k 2^{l_j\gamma_j^k} + \delta_j^k\right) \text{ if}\\ &l_j^{(d,k-1)} < l_j < l_j^{(d,k)}\end{aligned} \tag{18}$$

with $k \in \{1, 2, \ldots\ldots m^d\}$ and m^d is a given parameter corresponding to the number of intervals (i.e., the number of segments defined to approximate the distortion), where $\forall k \in \{1, 2, \ldots\ldots m^d\}$, $d_j^k > 0, \gamma_j^k > 0, \delta_j^k > 0$, and η_j are some weighting factors.

$$\upsilon_j = \left(\frac{1}{2} + \zeta_j\right)^{p_j+1} + \left(\frac{1}{2} - \zeta_j\right)^{p_j+1}$$

where $\zeta_j \in [-\frac{1}{2}, \frac{1}{2}]$ is an offset parameter indicating the shift of the reconstruction level with respect to the middle of the quantization interval. In this paper, our quantization rule corresponds to the case when ζ_j equals to 0 (i.e., mid-interval reconstruction). Therefore:

$$\upsilon_j = \left(\frac{1}{2}\right)^{p_j} \tag{19}$$

The values are also chosen in a way that the resulting function $d_j(l_j)$ is a good approximation $\left(l_j^{(d,k)}\right)_{1 \leq k \leq m^d}$ of the distortion. By taking $\gamma_j^1 = p_j$ and $\eta_j = d_j^1 = \frac{\upsilon_j}{p_j+1}$, we obtained the distortion $d_j(l_j) = \frac{\upsilon_j}{p_j+1} 2^{l_j p_j}$ on the first interval $\left[l_j^{(d,0)}, l_j^{(d,1)}\right]$, which corresponds to the classical asymptotic behavior of the distortion at high bit rate.

In this paper, we also used the Euclidean distance, which corresponds to $p_j = 2$ for each j. Therefore, $d_j(l_j) = \frac{\upsilon_j}{p_j+1} 2^{l_j p_j} = \frac{1}{p_j+1}\left(\frac{1}{2}\right)^{p_j} 2^{l_j p_j} = \frac{{\Delta_j}^2}{12}$ at high bit rate, which is a well-known asymptotic behavior.

We derived $(d_j^2, \gamma_j^2, \delta_j^2)$ such that $d_j(l_j)$ on the interval $\left[l_j^{(d,1)}, l_j^{(d,2)}\right]$ is tangent to the distortion function at an arbitrary point $l_j > l_j^{(d,1)}$. After that, the value of $l_j^{(d,1)}$ can be selected by identifying the configuration where the approximation error between the distortion function and the function $d_j(l_j)$ on the interval $\left[l_j^{(d,0)}, l_j^{(d,2)}\right]$ is small. By following the same strategy, we deduced the remaining values of $l_j^{(d,2)}, l_j^{(d,3)}, \ldots\ldots l_j^{(d,m^d-1)}$.

For a full wavelet decomposition of depth five, two sub-band nodes were chosen to illustrate histogram and rate-distortion curve approximations. **Figure 3** shows a subset of the histogram of wavelet packet sub-band coefficients compared to their estimated GGD, and **Figure 4** compares the operational rate-distortion curve with the approximate one obtained using the proposed piecewise affine method.

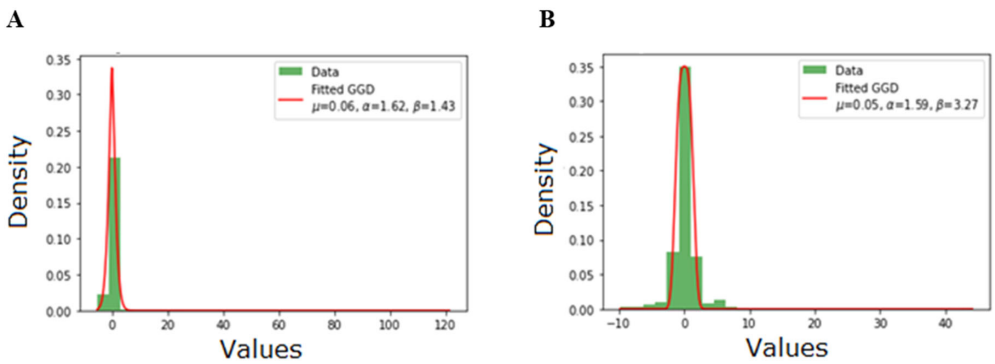

Figure 3. Comparison between the histogram of wavelet packet sub-band coefficients and their fitted generalized Gaussian distribution (GGD). (A) Sub-band 30. (B) Sub-band 60.

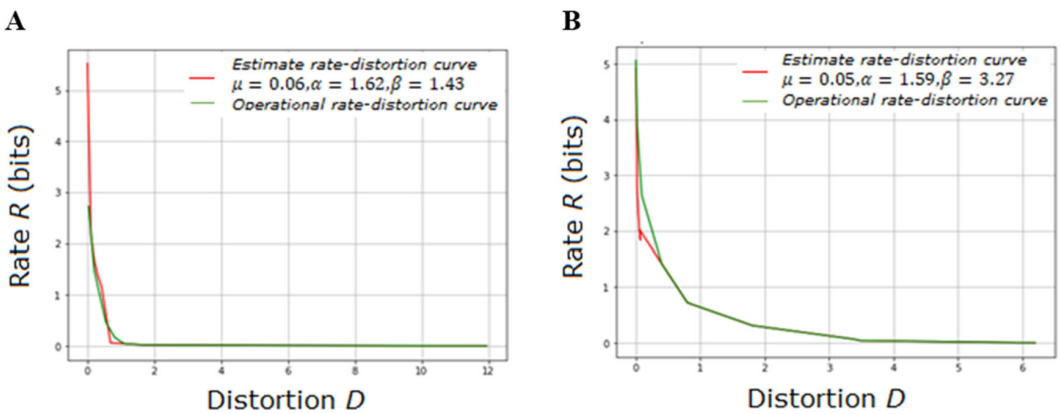

Figure 4. Operational rate-distortion curves versus the proposed piecewise affine approximations. (A) Sub-band 30. (B) Sub-band 60.

2.4. Scalar quantization and entropic coding

The scalar quantization step and entropy encoding are identical to those presented in a previous study.[36] However, it is necessary to send the information to the decoder based on the basis kept during the wavelet packet transformation. We chose to send an N-bit mask $(N = 2^L - 1)$. If the k-bit position is equal to 1, the number k sub-band is part of the decomposition. If the L value is high, a run-length encoding (RLE) is applied to the mask.

2.5. Performance metrics for the compression of the electromyography signals

To assess the performance of the proposed approach, the following metrics were used:

- CR: The ratio of the original data size to the compressed data size. An efficient compression is expected to have a high CR.

$$CR = \frac{Original\ size}{Compressed\ size} \tag{20}$$

- PRD: The root-mean-square (RMS) of the reconstruction error divided by the RMS of the original data. For a high-quality compression, the PRD is expected to be as low as possible.

$$PRD(\%) = 100\left(\frac{\sum_{i=0}^{i=N-1}(S_o(i) - S_r(i))^2}{\sum_{i=0}^{i=N-1}(S_o(i))^2}\right)^{\frac{1}{2}} \tag{21}$$

where S_o represents the original data, S_r represents the reconstructed data, and N is the number of data samples.

- SNR: Measuring the performance of compression algorithms implemented according to the widely used SNR criterion for assessing the numerical quality of the compression.

$$SNR = 10\log\left(\frac{\sum_{i=0}^{i=N-1}(S_o(i) - M)^2}{\sum_{i=0}^{i=N-1}(S_o(i) - S_r(i))^2}\right) \tag{22}$$

- QS: the ratio of CR to PRD. An efficient compression is expected to have a high QS.

3. Results and discussion

This section presents the experimental evaluation of the proposed frequency- and bit-rate-adaptive EMG compression method. Four EMG signals were considered: two surface EMG signals, denoted as 100s and v102s, and two needle EMG signals, denoted as emg_healthy and emg_myopathy.

The needle EMG signals correspond to healthy and myopathic muscle conditions, respectively. The original waveforms taken from the reference Non-Invasive Adaptive Prosthetics (NinaPro) database [35] are shown in **Figure 5**.

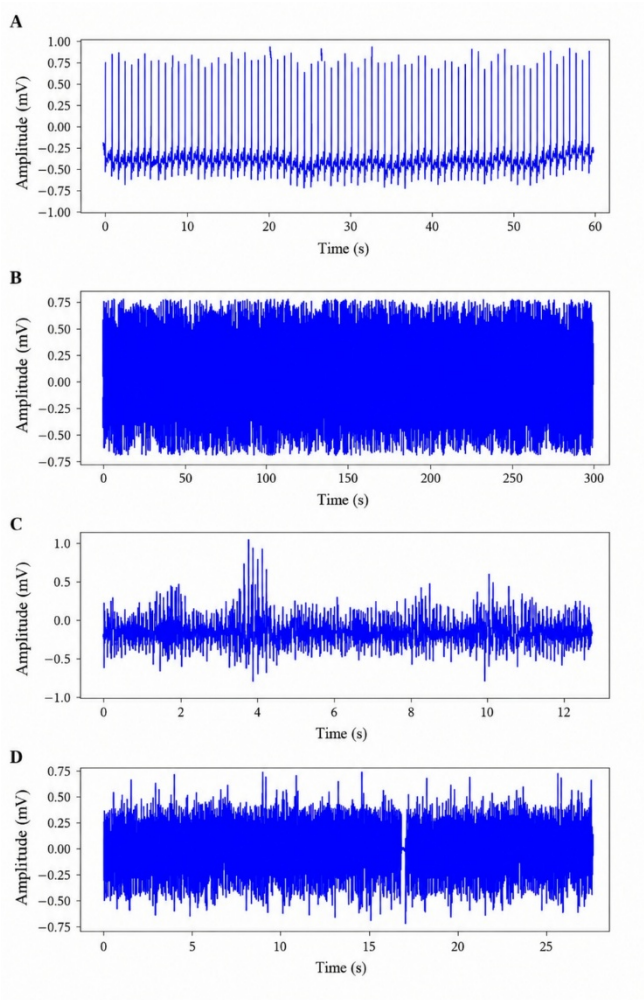

Figure 5. Original electromyography (EMG) signals used for experimentation. (A) Surface EMG 100s. (B) Surface EMG v102s. (C) Needle EMG emg_healthy. (D) Needle EMG emg_myopathy.

These signals provided different test conditions: 100s exhibited a more regular structure, v102s contained dense, high-frequency activity, and needle EMG signals showed more localized, irregular variations.

The proposed method was applied to a complete wavelet packet decomposition tree of depth L = 5. Two wavelet families were considered to evaluate the behavior of the method with different time–frequency bases: the orthogonal Daubechies db2 wavelet and the biorthogonal bior4.4 wavelet. The full wavelet packet decomposition tree and the wavelet functions are shown in **Figure 6**.

The reconstructed EMG signals obtained with the proposed adaptive method for a CR of 15 are presented in **Figure 7**.

The best bases selected by the proposed method for representative surface (100s) and needle (emg_healthy) EMG signals are shown in **Figures 8 and 9**, respectively. The quantitative results are reported in **Tables 1–4**. **Tables 1 and 2** report the results obtained for the surface EMG signals 100s and v102s, respectively, while **Tables 3 and 4** report those obtained for the needle EMG signals emg_healthy and emg_myopathy, respectively. To evaluate the effectiveness of the proposed approach, its reconstruction quality metrics were compared with those of a baseline wavelet-based compression method. The result comparisons are presented in **Figures 10–13**.

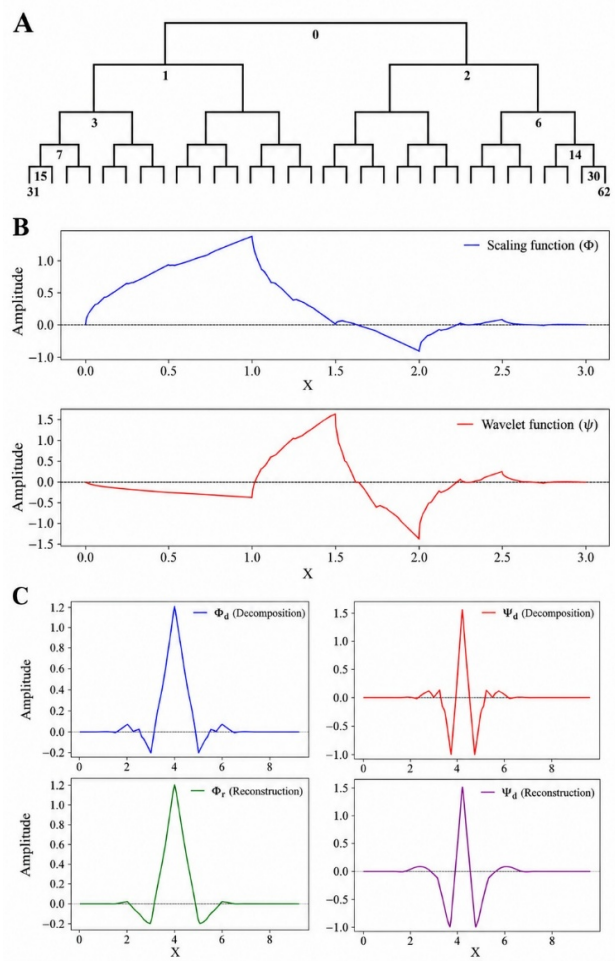

Figure 6. Wavelet packet decomposition tree and mother wavelet functions. (A) Full wavelet packet decomposition tree of depth five used to search for the best basis. (B) Orthogonal Daubechies db2 wavelet (scaling and wavelet functions). (C) Biorthogonal bior4.4 wavelet (scaling and wavelet functions).

3.1. Signal reconstruction quality analysis

The reconstructed signals shown in **Figure 7** provide a visual confirmation of the effectiveness of the proposed method. For the 100s signal, the reconstructed waveform preserved the main periodic structure and the dominant amplitude variations. This agrees with the low root-mean-square error (RMSE) and PRD values reported in **Table 1**. For v102s, the reconstructed signal also preserved the global dense activity pattern, but the error became more visible because the original signal contained stronger high-frequency variations. This explains the higher PRD values observed in **Table 2**.

For the needle EMG signals, the reconstruction quality depends strongly on the signal condition. In the emg_healthy case, the main bursts and amplitude variations were preserved reasonably well at a CR of 15. In the emg_myopathy case, the reconstructed waveform remained globally consistent with the original signal, but some local details were more affected by compression. This is expected because pathological EMG activity is more irregular and less sparse

in the selected transform domain. Therefore, the visual results and numerical metrics show the same trend: the proposed method preserves the dominant EMG structures, but reconstruction becomes more difficult for highly irregular and pathological signals when the CR increases.

It is also important to note that the proposed method did not provide the same level of improvement for all signals. The best gains were obtained when the wavelet packet representation concentrated most of the signal energy into a limited number of informative sub-bands. When the signal contained more distributed or irregular high-frequency content, as in v102s and emg_myopathy, the method still improved the rate-distortion trade-off, but the absolute reconstruction error remained higher.

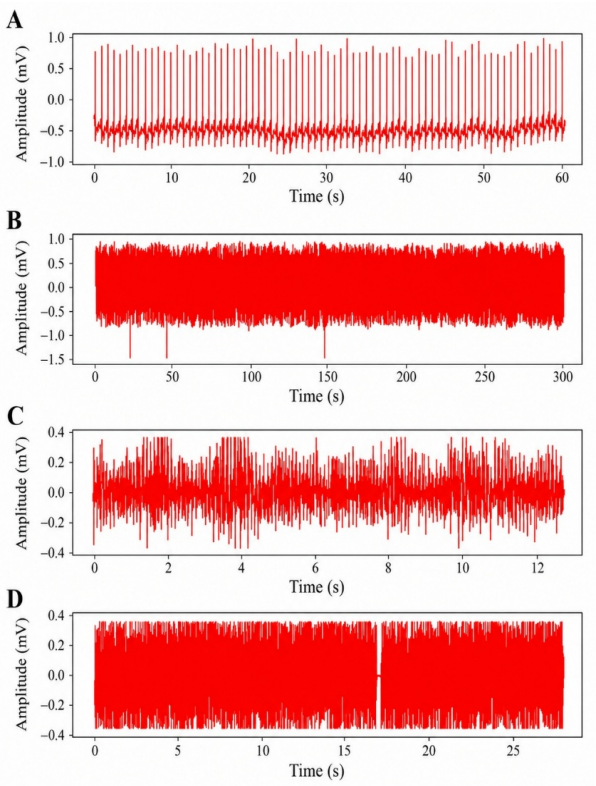

Figure 7. Reconstructed electromyography (EMG) signals using the proposed adaptive method at a compression ratio of 15. (A) Signal of 100s. (B) Signal of v102s. (V) Signal of emg_healthy. (D) Signal of emg_myopathy.

3.2. Best basis selection analysis

The results in **Figures 8 and 9** show that the proposed method did not use a fixed decomposition structure. Instead, the retained wavelet packet sub-bands changed according to both the signal characteristics and the target CR.

This behavior confirms the adaptive nature of the proposed approach. For the surface EMG signal 100s, the selected db2 basis changed from a compact representation using a small number of sub-bands at low CR to a deeper representation as the CR increased. For a CR of 15, the retained sub-bands were mainly concentrated in a reduced part of the tree, whereas at higher CRs, deeper nodes, such as 31 and 32, were selected. This indicates that the algorithm preserves the frequency regions that contribute most to the reconstruction quality while reducing the bit allocation in less informative regions. A similar behavior was observed for the needle EMG signal emg_healthy. With the bior4.4 wavelet, several sub-bands were repeatedly selected over different CRs, but their quantization precision decreased as the target CR increased. This result is important because it shows that the method adapts in two complementary ways. First, it selects the wavelet packet basis that provides the best rate-distortion compromise. Second, it assigns different quantization precisions to the retained sub-bands according to their relative importance. The bit-rate allocation algorithm, guided by rate-distortion analysis, proved effective at dynamically adjusting quantization precision across different wavelet packet sub-bands. This adaptiveness allowed the method to prioritize high-frequency components associated with transient EMG events while compressing less critical regions more aggressively. The performance gains from this adaptive nature are most pronounced in signals with high variability, where fixed-rate methods often struggle. Adaptive electrode shift correction methods[37] complement our frequency-adaptive approach by addressing sensor placement variability.

This behavior contrasts with the baseline wavelet-based method, which uses a fixed decomposition structure. In the baseline approach, the same set of sub-bands is retained independently of the signal and the target CR. As a result, the baseline cannot redistribute the bit budget according to the local frequency content of each EMG signal. The improvement obtained by the proposed method is therefore not only due to the wavelet packet transform itself, but also to the joint selection of the best basis and the optimal scalar quantizer bit rates.

3.3. Quantitative and comparative analysis

The quantitative results in **Tables 1–4** show the expected trade-off between compression efficiency and reconstruction quality.

When the CR increased, the number of available bits decreased, generally leading to higher RMSE and PRD values and lower SNR values. However, for almost all tested signals, the proposed adaptive method provided better reconstruction quality than the baseline wavelet-based method at the same CR.

For the surface EMG signal 100s, the proposed method achieved excellent reconstruction quality over the whole range of CRs. At a CR of 5, the best proposed configuration was obtained with bior4.4, with an RMSE of 0.4996, an SNR of 36.9396 dB, a PRD of 0.0522%, and a QS of 95.82. In comparison, the best baseline configuration achieved an RMSE of 0.9558, an SNR of 31.3046 dB, a PRD of 0.0998%, and a QS of 50.10. The gain remained visible at higher CRs. At a CR of 25, the proposed bior4.4 configuration achieved an RMSE of 2.6008 and an SNR of 22.6097 dB, whereas the best baseline configuration achieved an RMSE of 4.2531 and an SNR of 18.3377 dB. This confirms that the proposed method is particularly effective for signals whose energy can be efficiently represented by a small number of adapted wavelet packet sub-bands.

For the surface EMG signal v102s, the reconstruction task was more difficult because the signal contained dense and rapidly varying activity. This is reflected by larger RMSE and PRD values compared with 100s. Nevertheless, the proposed method still provided clear improvements over the baseline. At a CR of 15, the best proposed result was obtained with bior4.4, with an RMSE of 72.7398, an SNR of 19.8658 dB, a PRD of 10.1273%, and a QS of 1.48. The best baseline result at the same CR achieved an RMSE of 134.1810, an SNR of 14.5474 dB, a PRD of 18.6815%, and a QS of 0.80. This shows that adaptive selection of the basis and bit-allocation strategy are useful even when the signal has broad and complex frequency content.

Table 1. Reconstruction quality metrics for the surface electromyography signal 100s

CR	Wavelet	Sub-bands	Precision	RMSE	SNR (dB)	PRD (%)	QS
5	Daubechies db2	[1 5 6]	[9 7 8]	0.7396	33.5323	0.0772	64.73
	Bior4.4	[3 9 12 13 21 22 23 24 59 60 61 62]	[9 8 7 8 8 9 7 5 6 8 9 9]	0.4996	36.9396	0.0522	95.82
10	Baseline db2	[0 1 2 3 4 5]	[9 9 9 9 9 7]	0.9558	31.3046	0.0998	50.10
	Baseline bior4.4	[0 1 2 3 4 5]	[9 9 9 9 9 9]	1.3324	28.4189	0.1392	35.93
	Daubechies db2	[4 5 6 8 15 16]	[8 5 6 8 9 9]	1.2555	28.9357	0.1311	76.26
	Bior4.4	[2 7 8 9 10]	[8 9 9 7 9]	1.3824	28.0994	0.1444	69.26
	Baseline db2	[0 1 2 3 4 5]	[8 9 8 7 7 6]	1.8507	25.5653	0.1933	51.73
	Baseline bior4.4	[0 1 2 3 4 5]	[9 9 9 9 8 7]	1.8330	25.6486	0.1915	52.23
15	Daubechies db2	[2 4 8 15 16]	[2 7 7 9 8]	1.8800	25.4289	0.1964	76.39
	Bior4.4	[2 8 9 15 16 21 22]	[6 9 5 9 9 6 8]	1.6988	26.3091	0.1774	84.55
	Baseline db2	[0 1 2 3 4 5]	[7 8 7 6 6 5]	2.5264	22.8619	0.2639	56.84
	Baseline bior4.4	[0 1 2 3 4 5]	[9 9 8 8 7 5]	2.3460	23.5052	0.2450	61.21
20	Daubechies db2	[4 5 6 8 16 31 32]	[6 4 3 7 8 9 8]	2.3508	23.4875	0.2455	81.45
	Bior4.4	[2 4 8 15 16]	[6 7 8 9 9]	2.1401	24.3031	0.2235	89.47
	Baseline db2	[0 1 2 3 4 5]	[7 7 6 6 5 2]	3.1882	20.8409	0.3330	60.06
	Baseline bior4.4	[0 1 2 3 4 5]	[8 8 7 7 6 6]	3.2659	20.6319	0.3411	58.63
25	Daubechies db2	[2 4 8 16 31 32]	[3 6 6 7 9 8]	3.3564	20.3943	0.3506	71.31
	Bior4.4	[2 4 8 16 31 32]	[6 7 7 8 9 8]	2.6008	22.6097	0.2717	92.03
	Baseline db2	[0 1 2 3 4 5]	[6 6 6 5 4 4]	4.2531	18.3377	0.4443	56.27
	Baseline bior4.4	[0 1 2 3 4 5]	[8 7 7 6 5 6]	4.2725	18.2983	0.4463	56.02

Abbreviations: CR: Compression ratio; PRD: Percentage root-mean-square difference; QS: Quality score; RMSE: Root-mean-square error; SNR: Signal-to-noise ratio.

Table 2. Reconstruction quality metrics for the surface electromyography signal v102s

CR	Wavelet	Sub-bands	Precision	RMSE	SNR (dB)	PRD (%)	QS
5	Daubechies db2	[2 4 8 31 32 33 34]	[9 8 9 9 9 9 9]	11.5494	35.8500	1.6080	3.11
	Bior4.4	[2 4 8 16 31 32]	[9 9 9 9 9 8]	17.6390	32.1717	2.4558	2.04
	Baseline db2	[0 1 2 3 4 5]	[8 8 8 7 6 9]	19.9209	31.1150	2.7735	1.80
	Baseline bior4.4	[0 1 2 3 4 5]	[8 7 7 8 7 9]	17.8031	32.0913	2.4787	2.02
10	Daubechies db2	[2 4 8 15 16]	[7 5 6 7 8]	37.7404	25.5651	5.2545	1.90
	Bior4.4	[2 4 8 31 32 33 34]	[7 6 7 6 6 7 6]	40.1014	25.0380	5.5832	1.79
	Baseline db2	[0 1 2 3 4 5]	[6 6 6 5 4 6]	70.4520	20.1433	9.8088	1.02
	Baseline bior4.4	[0 1 2 3 4 5]	[7 6 6 5 4 6]	76.0713	19.4768	10.5912	0.94
15	Daubechies db2	[2 4 8 16 31 32]	[6 4 5 6 5 5]	76.3136	19.4492	10.6249	1.41
	Bior4.4	[2 4 8 31 32 33 34]	[7 4 5 5 5 6 5]	72.7398	19.8658	10.1273	1.48
	Baseline db2	[0 1 2 3 4 5]	[5 5 5 3 3 5]	138.5800	14.2672	19.2941	0.78
	Baseline bior4.4	[0 1 2 3 4 5]	[6 4 5 4 3 5]	134.1810	14.5474	18.6815	0.80
20	Daubechies db2	[2 4 8 15 16]	[6 3 4 5 5]	140.8360	14.1269	19.6082	1.02
	Bior4.4	[2 4 8 31 32 33 34]	[6 4 4 5 4 4 4]	115.5230	15.8478	16.0839	1.24
	Baseline db2	[0 1 2 3 4 5]	[4 4 4 3 2 5]	216.9530	10.3739	30.2057	0.66
	Baseline bior4.4	[0 1 2 3 4 5]	[4 3 4 3 3 5]	198.0160	11.1672	27.5692	0.73
25	Daubechies db2	[2 4 8 15 16]	[5 2 3 5 5]	181.7700	11.9107	25.3073	0.99
	Bior4.4	[2 4 8 31 32 33 34]	[5 3 4 4 4 4 4]	179.8740	12.0018	25.0433	1.00
	Baseline db2	[0 1 2 3 4 5]	[5 4 4 3 2 4]	300.7720	7.5365	41.8755	0.60
	Baseline bior4.4	[0 1 2 3 4 5]	[4 3 3 3 2 5]	261.9900	8.7355	36.4761	0.69

Abbreviations: CR: Compression ratio; PRD: Percentage root-mean-square difference; QS: Quality score; RMSE: Root-mean-square error; SNR: Signal-to-noise ratio.

For the needle EMG signal emg_healthy, the proposed method also outperformed the baseline over the tested CRs. At a CR of 5, the bior4.4-based adaptive configuration achieved an RMSE of 7.1825, an SNR of 41.1058 dB, a PRD of 0.8805%, and a QS of 5.68. In contrast, the best baseline configuration achieved an RMSE of 20.4118, an SNR of 32.0337 dB, a PRD of 2.5022%, and a QS of 2.00. At a CR of 15, the proposed bior4.4 configuration still provided a better compromise, with an RMSE of 68.9595 and an SNR of 21.4594 dB, compared with an RMSE of 103.6260 and an SNR of 17.9219 dB for the best baseline configuration.

For the needle EMG signal emg_myopathy, the compression problem was more challenging. This signal contained irregular and pathological activity. Even in this case, the proposed method remained globally better than the baseline when the best adaptive configuration was considered (**Figures 10–13**). At a CR of 15, the proposed bior4.4 configuration achieved an RMSE of 209.8640, an SNR of 13.2993 dB, a PRD of 21.6288%, and a QS of 0.69. The best baseline result achieved an RMSE of 280.3110, an SNR of 10.7853 dB, a PRD of 28.8891%, and a QS of 0.52. At a CR of 20, the db2 adaptive configuration became less favorable, but the

bior4.4 adaptive configuration still improved the reconstruction quality compared with the baseline. This observation shows that the choice of the mother wavelet can influence the final performance, especially for pathological or highly irregular EMG signals.

Recent transformer-based EMG compression[38] achieves comparable metric improvements under similar test conditions. The effect of mother wavelet selection on compression performance is an important aspect that was not extensively explored in this study. Different wavelet families, such as Symlets, Coiflets, and biorthogonal wavelets, offer varying time–frequency localization properties that may affect both the energy compaction and the sparsity of wavelet packet coefficients. In principle, selecting the optimal mother wavelet could be integrated into the overall optimization framework, jointly with the best-basis selection and bit-allocation strategy. However, such an extension would significantly increase the computational complexity, as it would require exploring multiple wavelet families in addition to the already large wavelet packet basis tree. Therefore, in this work, the mother wavelet was fixed to maintain a reasonable computational cost. Future investigations will consider efficient strategies for joint optimization, aiming to balance performance gains with computational constraints in practical implementations.

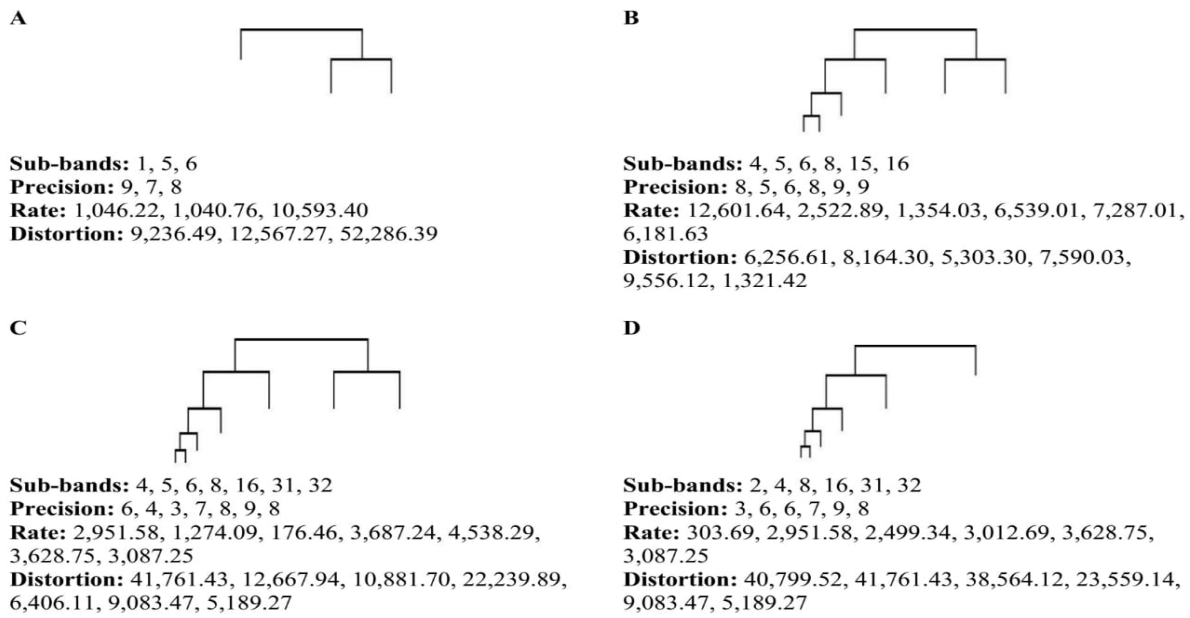

Figure 8. Best wavelet packet basis selected by the proposed method for surface EMG signal 100s using the Daubechies db2 wavelet at different compression ratios (CR): (A) CR = 5, (B) CR = 15, (C) CR = 20, and (D) CR = 25.

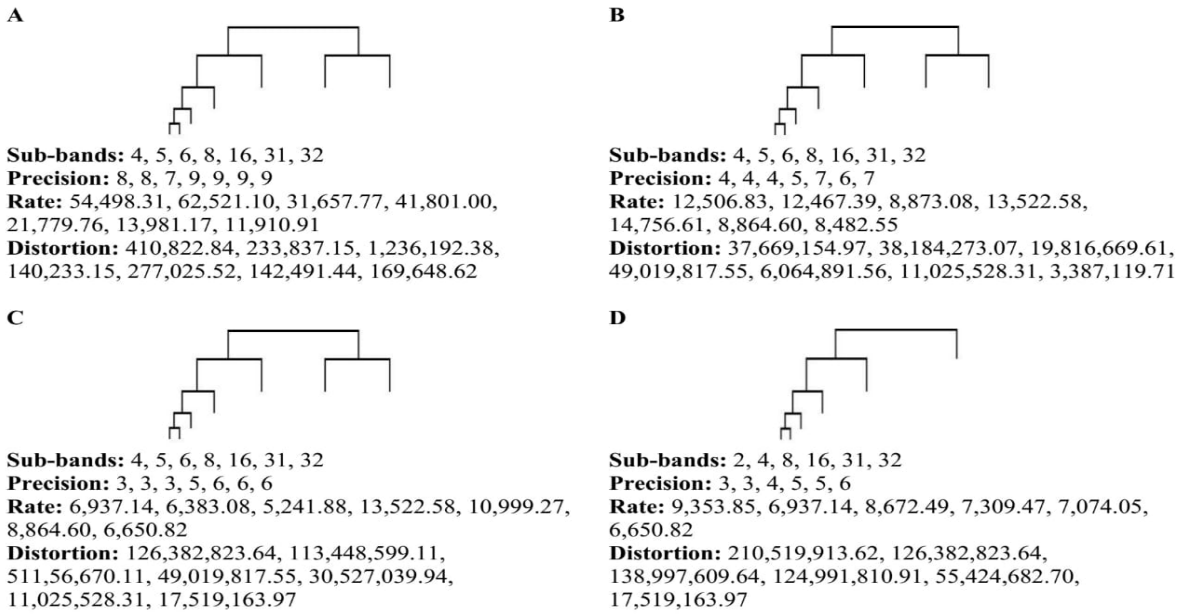

Figure 9. Best wavelet packet basis selected by the proposed method for needle EMG signal emg_healthy using the Bior4.4 wavelet at different compression ratios (CRs): (A) CR = 5, (B) CR = 15, (C) CR = 20, and (D) CR = 25.

Table 3. Reconstruction quality metrics for the needle electromyography signal emg_healthy

CR	Wavelet	Sub-bands	Precision	RMSE	SNR (dB)	PRD (%)	QS
5	Daubechies db2	[4 6 8 11 12 16 31 32]	[8 7 9 7 7 9 9 9]	7.5200	40.7070	0.9218	5.42
	Bior4.4	[4 5 6 8 16 31 32]	[8 8 7 9 9 9 9]	7.1825	41.1058	0.8805	5.68
	Baseline db2	[0 1 2 3 4 5]	[9 9 8 8 6 6]	21.6220	31.5333	2.6505	1.89
	Baseline bior4.4	[0 1 2 3 4 5]	[9 9 9 8 6 6]	20.4118	32.0337	2.5022	2.00
10	Daubechies db2	[4 5 6 8 16 31 32]	[5 5 5 7 8 8 7]	36.1668	27.0651	4.4335	2.26
	Bior4.4	[4 5 6 8 16 31 32]	[7 5 6 7 8]	30.9868	28.4077	3.7985	2.63
	Baseline db2	[0 1 2 3 4 5]	[8 6 7 5 4 4]	65.2754	21.9363	8.0018	1.25
	Baseline bior4.4	[0 1 2 3 4 5]	[8 7 7 5 4 4]	58.8735	22.8329	7.2127	1.39
15	Daubechies db2	[4 5 6 8 16 31 32]	[4 4 4 5 7 6 6]	78.9486	20.2844	9.6779	1.55
	Bior4.4	[4 5 6 8 16 31 32]	[4 4 4 5 7 6 7]	68.9595	21.4594	8.4534	1.77
	Baseline db2	[0 1 2 3 4 5]	[7 6 6 4 3 3]	111.2870	17.3024	13.6421	1.10
	Baseline bior4.4	[0 1 2 3 4 5]	[7 7 6 4 3 3]	103.6260	17.9219	12.7029	1.18
20	Daubechies db2	[2 4 8 16 31 32]	[3 3 5 6 6 5]	108.4810	17.5242	13.2981	1.50
	Bior4.4	[4 5 6 8 16 31 32]	[3 3 3 5 6 6 6]	108.5420	17.5193	13.3056	1.50
	Baseline db2	[0 1 2 3 4 5]	[5 6 5 4 3 2]	142.2690	15.1691	17.4399	1.15
	Baseline bior4.4	[0 1 2 3 4 5]	[6 5 5 4 3 2]	141.6500	15.2069	17.3641	1.15
25	Daubechies db2	[2 4 8 16 31 32]	[3 3 4 5 5 5]	156.9700	14.3150	19.2420	1.30
	Bior4.4	[2 4 8 16 31 32]	[3 3 4 5 5 6]	147.8820	14.8329	18.1281	1.38
	Baseline db2	[0 1 2 3 4 5]	[5 4 5 4 2 2]	178.9520	13.1765	21.9367	1.14
	Baseline bior4.4	[0 1 2 3 4 5]	[6 5 5 3 2 2]	172.7390	13.4835	21.1751	1.18

Abbreviations: CR: Compression ratio; PRD: Percentage root-mean-square difference; QS: Quality score; RMSE: Root-mean-square error; SNR: Signal-to-noise ratio.

Table 4. Reconstruction quality metrics for the needle electromyography signal emg_myopathy

CR	Wavelet	Sub-bands	Precision	RMSE	SNR (dB)	PRD (%)	QS
5	Daubechies db2	[4 5 6 7 8]	[6 7 7 8 7]	21.3129	33.1652	2.1965	2.28
	Bior4.4	[4 5 6 7 8]	[7 7 6 8 7]	20.7720	33.3885	2.1408	2.34
	Baseline db2	[0 1 2 3 4 5]	[9 8 7 6 5 5]	62.9559	23.7583	6.4883	0.77
	Baseline bior4.4	[0 1 2 3 4 5]	[8 6 7 6 6 5]	62.1643	23.8672	6.4067	0.78
10	Daubechies db2	[4 6 8 1 12 15 16]	[4 5 5 4 4 6 5]	116.3570	18.4222	11.9919	0.83
	Bior4.4	[4 5 6 8 15 16]	[4 5 4 5 6 6]	111.5120	18.7917	11.4925	0.87
	Baseline db2	[0 1 2 3 4 5]	[6 5 5 4 4 3]	202.1720	13.6236	20.8361	0.48
	Baseline bior4.4	[0 1 2 3 4 5]	[7 5 6 4 4 3]	201.6860	13.6445	20.7860	0.48
15	Daubechies db2	[4 5 6 7 8]	[3 3 4 5 4]	224.6820	12.7067	23.1560	0.65
	Bior4.4	[4 5 6 7 8]	[4 4 45 7]	209.8640	13.2993	21.6288	0.69
	Baseline db2	[0 1 2 3 4 5]	[5 4 4 4 2 3]	302.6440	10.1194	31.1908	0.48
	Baseline bior4.4	[0 1 2 3 4 5]	[6 4 4 3 3 3]	280.3110	10.7853	28.8891	0.52
20	Daubechies db2	[2 8 9 10 16 31 32]	[3 3 3 3 4 5 4]	396.2010	7.7798	40.8328	0.49
	Bior4.4	[4 5 6 8 15 16]	[3 3 4 5 4]	258.4900	11.4892	26.6402	0.75
	Baseline db2	[0 1 2 3 4 5]	[6 5 4 3 2 2]	376.6240	8.2199	38.8152	0.52
	Baseline bior4.4	[0 1 2 3 4 5]	[6 4 5 3 2 2]	380.8220	8.1236	39.2479	0.51
25	Daubechies db2	[5 6 8 9 10 16 31 32]	[2 3 3 2 3 4 5 4]	366.1240	8.4655	37.7331	0.66
	Bior4.4	[4 5 6 7 8]	[3 3 2 4 3]	314.4970	9.7857	32.4123	0.77
	Baseline db2	[0 1 2 3 4 5]	[4 4 3 3 2 2]	415.7400	7.3616	42.8466	0.58
	Baseline bior4.4	[0 1 2 3 4 5]	[5 4 3 3 2 2]	415.6460	7.3636	42.8369	0.58

Abbreviations: CR: Compression ratio; PRD: Percentage root-mean-square difference; QS: Quality score; RMSE: Root-mean-square error; SNR: Signal-to-noise ratio.

3.4. Influence of the wavelet family

The quantitative comparisons of reconstruction quality metrics (RMSE, SNR, PRD, and QS) between the proposed adaptive method and the baseline wavelet-based method are illustrated in **Figures 10** (100s), **11** (v102s), **12** (emg_healthy), and **13** (emg_myopathy). The comparison between Daubechies db2 and bior4.4 showed that no single mother wavelet was optimal for all signals and all CRs. For the 100s signal, bior4.4 provided the best performance for most CRs, except at a CR of 10, where db2 achieved a slightly better result. For v102s, db2 performed better at low CRs, whereas bior4.4 became more favorable at medium and high CRs. For the needle EMG signals, bior4.4 generally provides the best reconstruction quality, especially for emg_myopathy.

These results suggest that the proposed optimization framework is able to benefit from the properties of the selected wavelet family, but the mother wavelet still has an influence on the final compression performance. The biorthogonal bior4.4 wavelet appeared particularly effective for several tested cases, probably because its reconstruction properties provide a better compromise for preserving local waveform structures. However, the results also show that db2 remained competitive in some configurations. A systematic optimization of the mother wavelet could further improve

the method, but it would also increase computational cost, as several wavelet packet dictionaries would need to be explored.

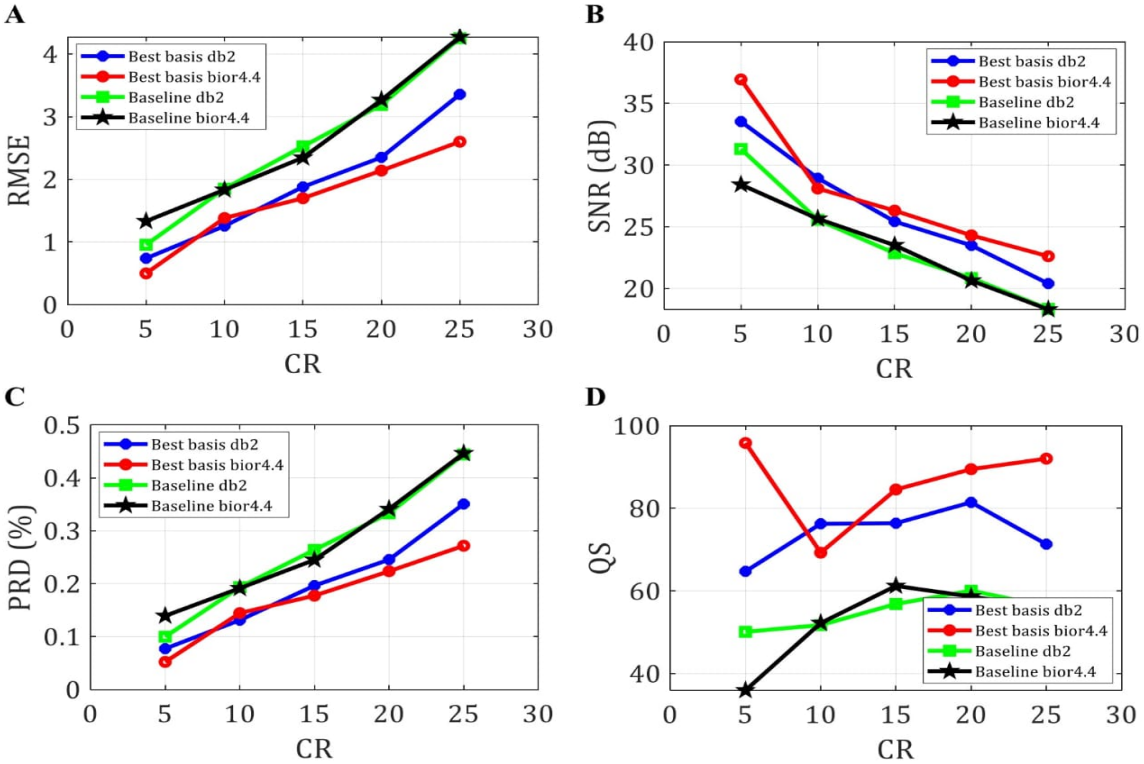

Figure 10. Comparison of reconstruction quality metrics for surface electromyography signal 100s across all tested compression ratios (CRs) and configurations: (A) root-mean-square error (RMSE), (B) signal-to-noise ratio (SNR), (C) percentage root-mean-square difference (PRD), and (D) quality score (QS).

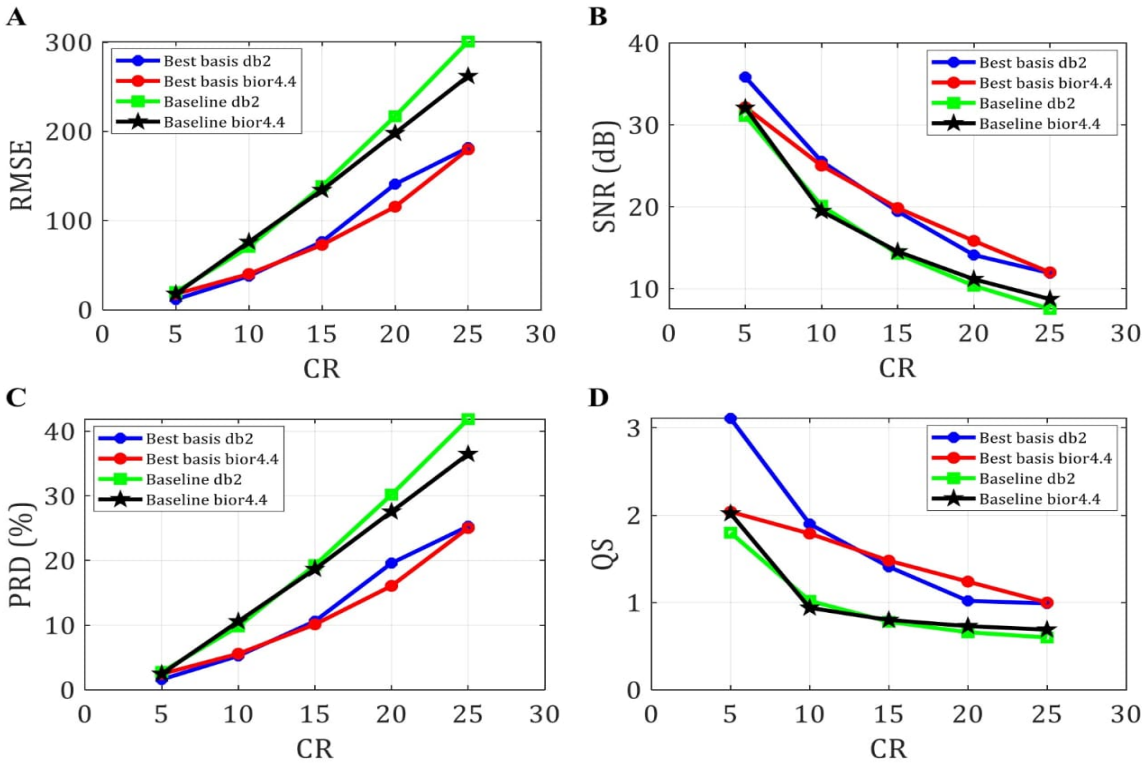

Figure 11. Comparison of reconstruction quality metrics for surface electromyography signal v102s across all tested compression ratios (CRs) and configurations: (A) root-mean-square error (RMSE), (B) signal-to-noise ratio (SNR), (C) percentage root-mean-square difference (PRD), and (D) quality score (QS).

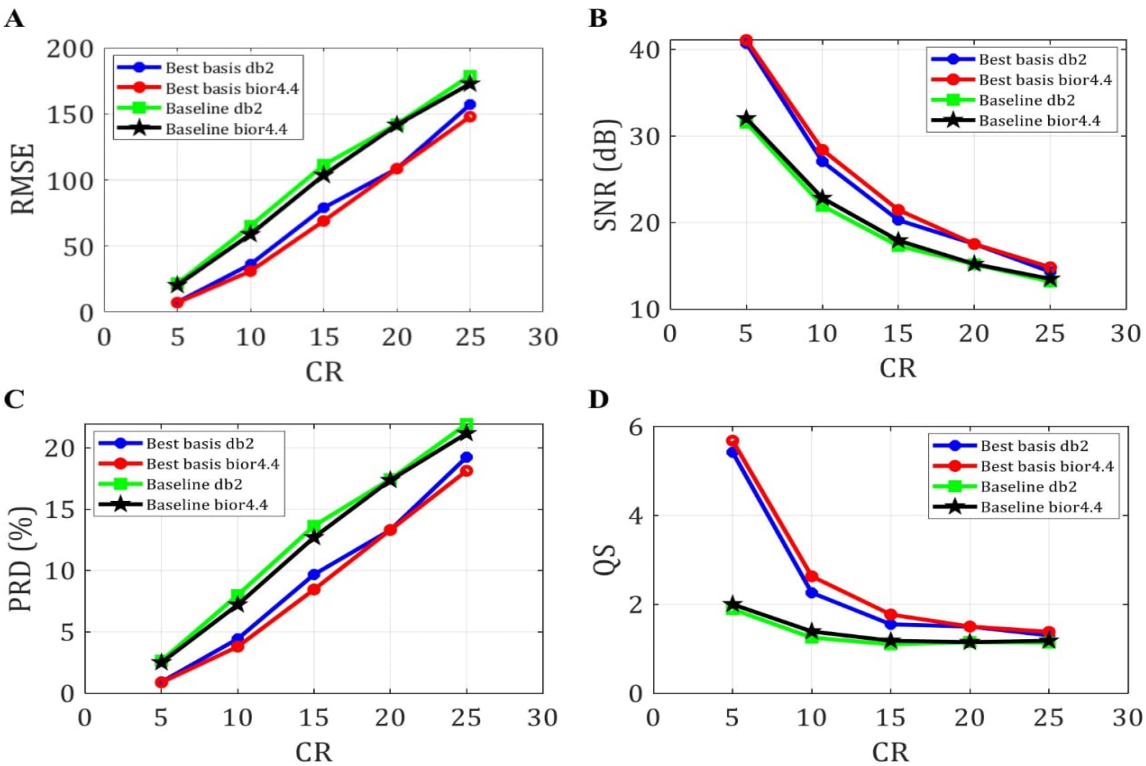

Figure 12. Comparison of reconstruction quality metrics for needle electromyography signal emg_healthy across all tested compression ratios (CRs) and configurations: (A) root-mean-square error (RMSE), (B) signal-to-noise ratio (SNR), (C) percentage root-mean-square difference (PRD), and (D) quality score (QS).

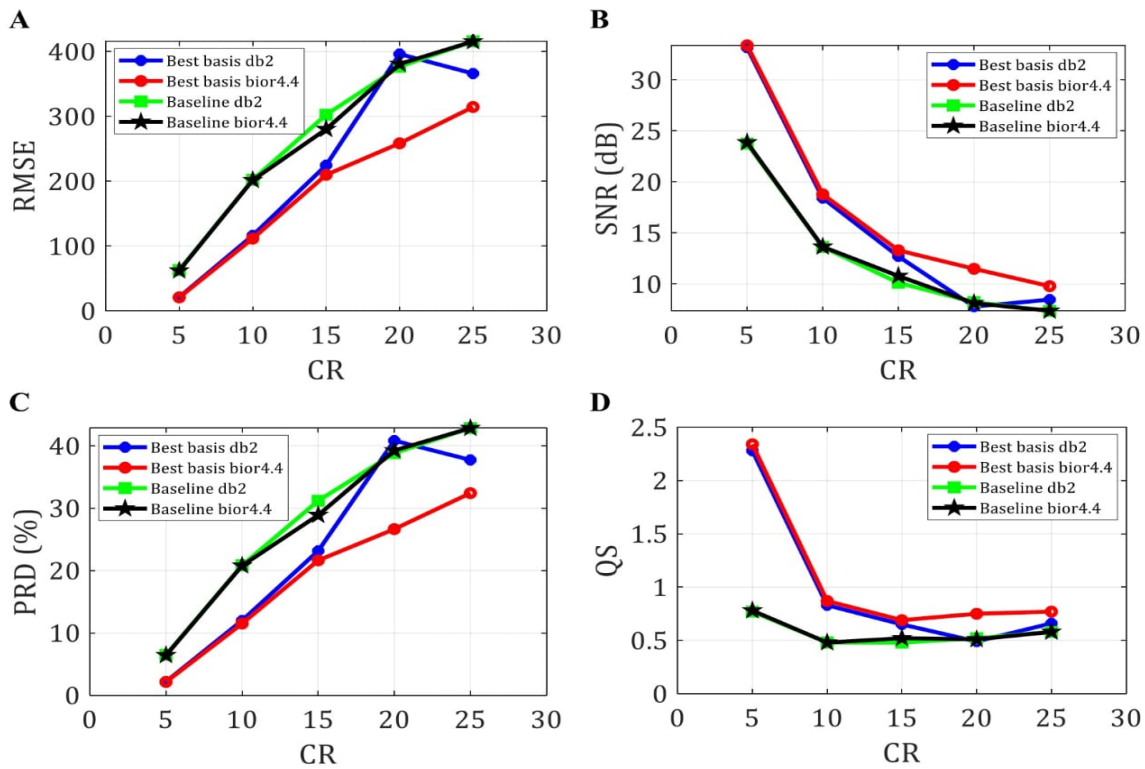

Figure 13. Comparison of reconstruction quality metrics for needle electromyography signal emg_myopathy across all tested compression ratios (CRs) and configurations: (A) root-mean-square error (RMSE), (B) signal-to-noise ratio (SNR), (C) percentage root-mean-square difference (PRD), and (D) quality score (QS).

4. Discussion and limitations

The improved performance of the proposed method can be explained by the combination of three elements. First, the wavelet packet transform provides a richer set of admissible bases than the conventional wavelet transform. Second, the rate-distortion criterion allows the method to select the basis that best balances compression efficiency and reconstruction quality. Third, the optimal allocation of scalar quantizer bit rates gives more precision to the most informative sub-bands and reduces the number of bits assigned to less relevant components. Unlike fixed-basis methods, which may overlook significant signal details, the adaptive method tailors the compression process to each signal's unique structure and bit rate target. This capability makes it particularly suitable for real-time applications, such as prosthetic control and remote healthcare monitoring, where both high compression efficiency and fidelity are crucial. Patch-based transformer–convolutional neural network architectures[39] offer alternative sparsity-exploitation strategies that can be combined with our wavelet packet basis selection. Despite its advantages, the computational complexity of the proposed method, primarily due to the wavelet packet transform and rate-distortion analysis, is higher than that of traditional methods.

The proposed method relies on the GGD to model the statistical distribution of wavelet packet sub-band coefficients. While this model is widely adopted due to its flexibility and analytical tractability, its accuracy may degrade in the presence of strong noise or low SNR conditions. In such cases, the estimated GGD parameters may no longer accurately capture the true distribution of the coefficients, thereby affecting the precision of the rate-distortion approximation. This limitation is particularly relevant for EMG signals affected by motion artifacts, external interference, or severe physiological noise, where the sparsity assumptions underlying the wavelet representation may be weakened.

Regarding generalization, the current study was primarily validated on surface EMG (sEMG) signals. However, to further assess the robustness of the proposed approach, additional experiments were conducted on a set of pathological EMG signals (emg_myopathy) and needle EMG recordings, as reported in **Tables 3 and 4**. The obtained results are promising, indicating that the method remains effective beyond standard sEMG recordings, despite the increased complexity and variability of these signals. Nevertheless, these additional evaluations remain preliminary and do not yet cover the full diversity of pathological conditions or acquisition protocols. To further strengthen the generalization capability of the method, future work will extend the evaluation to larger and more diverse pathological and needle EMG datasets, as well as systematically investigate performance under low-SNR conditions. From a modeling perspective, more robust statistical representations may also be explored, including mixture models and noise-aware parameter estimation strategies. In addition, preprocessing techniques, such as denoising and artifact removal, could be integrated to improve the reliability of coefficient modeling in challenging acquisition environments.

Despite its performance advantages, the proposed method involves several computational steps, including wavelet packet decomposition, rate-distortion curve estimation, and Lagrangian optimization. However, a key contribution of this work lies in the reduction of computational complexity through the use of closed-form approximations of the rate–distortion function, thereby avoiding computationally expensive operational evaluations. This approach significantly reduces the overall processing burden compared to conventional methods that rely on exhaustive rate-distortion computations, making the proposed scheme more suitable for practical implementations. Future work could focus on optimizing these processes to enhance real-time applicability. From an implementation perspective, the proposed algorithm can be adapted to resource-constrained environments, such as embedded or portable EMG acquisition systems. Several optimization strategies may be employed, including the use of fixed-point arithmetic, precomputing and storing rate-distortion parameters in lookup tables, and limiting the depth of the wavelet packet decomposition tree to reduce computational load. In addition, simplified quantization parameter selection schemes can be designed to alleviate the complexity of the Lagrangian optimization stage. These strategies are consistent with lightweight design principles commonly adopted in microcontroller-based systems and constitute a promising pathway toward real-time implementation.

Moreover, the performance of the method on other biomedical signals, such as EEG or ECG, could be explored to extend its utility. In summary, compared to data-driven approaches such as deep learning-based compression methods, the proposed scheme does not require a training phase and is characterized by relatively low computational complexity, making it well-suited for real-time and resource-constrained applications. Although learning-based methods may achieve higher compression performance under certain conditions, they generally entail greater implementation complexity and reduced interpretability. In this context, the proposed approach can be viewed as occupying an intermediate position between classical transform-based techniques and modern data-driven paradigms, thereby offering a practical, efficient, and interpretable solution for EMG signal compression.

5. Conclusion

This study presented a frequency- and bit-rate-adaptive compression scheme for EMG signals, leveraging wavelet packet transforms, adaptive bit-rate allocation, and rate-distortion analysis. The proposed method demonstrated superior performance in achieving high CRs while preserving critical signal features, outperforming conventional wavelet-based compression techniques. By adaptively tailoring the compression strategy to the signal's frequency characteristics and the bit rate target, the method effectively minimized distortion, making it suitable for applications requiring high fidelity, such as prosthetic control and telemedicine. The results highlight the potential of the frequency- and bit-rate-adaptive approach in addressing the challenges of efficient storage and transmission of biomedical signals. The integration of GGD modeling further enhanced the quantization accuracy, particularly in handling non-stationary signal regions. Emerging spiking neural network architectures[40] could further reduce computational complexity while maintaining compression fidelity. Despite its computational complexity, the method provides a robust framework for balancing compression efficiency and signal integrity. The proposed method achieves a balanced trade-off between compression efficiency, signal fidelity, and computational complexity. By integrating adaptive wavelet packet decomposition with analytical rate-distortion optimization, it provides a robust and interpretable framework for EMG signal compression. Although the current validation is limited to a

subset of EMG signals, the proposed methodology demonstrates strong potential for extension to a broader range of biomedical signals and for deployment in embedded systems. Future work will focus on enhancing robustness in noisy environments, expanding experimental validation across diverse signal databases, and optimizing the implementation for real-time processing constraints.

Acknowledgments

None.

Funding

None.

Conflict of interest

The authors declare no conflict of interest.

Author contribution

Conceptualization: Joseph Mvogo Ngono
Formal analysis: All authors
Methodology: All authors
Software: Joseph Mvogo Ngono
Supervision: Auguste Noumsi Woguia, Christophe Lessouga Etoundi, Zeric Tabekoueng Njitacke, Pierre Ele
Validation: Joseph Mvogo Ngono
Writing–original draft: Joseph Mvogo Ngono, Arnaud Nanfak, Jean de Dieu Nkapkop

Availability of data

The data that support the findings of this study are available from the corresponding author upon reasonable request.

AI tools statement

The authors confirm that no AI tools were utilized in this work and the preparation of this manuscript.

References

1. Biagetti G, Crippa P, Falaschetti L, Mansour A, Turchetti C. Energy and performance analysis of lossless compression algorithms for wireless EMG sensors. *Sensors*. 2021;21(15):5160. https://doi.org/10.3390/s21155160
2. Gupta A, Bansal A, Khanduja V. Modern lossless compression techniques: review, comparison and analysis. In: *2017 Second International Conference on Electrical, Computer and Communication Technologies (ICECCT)*. IEEE; 2017:1-8. https://doi.org/10.1109/ICECCT.2017.8117850
3. Ntsama PE, Welba C, Ele P. Comparison study of EMG signals compression by methods transform using vector quantization, SPIHT and arithmetic coding. *SpringerPlus*. 2016;5:444. https://doi.org/10.1186/s40064-016-2095-7
4. Elakkiya S, Thivya KS. Comprehensive review on lossy and lossless compression techniques. *J Inst Eng India Ser B*. 2022;103:1003-1012. https://doi.org/10.1007/s40031-021-00686-3
5. Subasi A. Classification of EMG signals using combined features and soft computing techniques. *Appl Soft Comput*. 2012;12(8):2188-2198. https://doi.org/10.1016/j.asoc.2012.03.035
6. Arias Correa JD, Roschildt Pinto AS, Montez C. Lossy data compression for IoT sensors: a review. *Internet Things*. 2022;19:100516. https://doi.org/10.1016/j.iot.2022.100516
7. Wang K, Bai Y, Li D, Zhai D, Jiang J, Liu X. Learning lossless compression for high bit-depth volumetric medical images. *IEEE Trans Image Process*. 2025;34:113-125. https://doi.org/10.1109/TIP.2024.3513156
8. Shuvo SB, Alam SS, Ayman SU, et al. Application of wavelet transformation and artificial intelligence techniques in healthcare: a systematic review. *WIREs Data Min Knowl Discov*. 2025;15:e70007. https://doi.org/10.1002/widm.70007
9. Gao J, Wang B, Wang Z, Wang Y, Kong F. A wavelet transform-based image segmentation method. *Optik*. 2020;208:164123. https://doi.org/10.1016/j.ijleo.2019.164123
10. Legendre S, Massicotte D, Goyette J, Bose TK. Wavelet-transform-based method of analysis for Lamb-wave ultrasonic NDE signals. *IEEE Trans Instrum Meas*. 2000;49(3):524-530. https://doi.org/10.1109/19.850388
11. Lal B, Ajbani M, Sodhro AH, Gravina R, O'Keeffe D. Efficient ECG compression and reconstruction via deep compressive sensing and hardware-efficient models. *Array*. 2026;30:100791. https://doi.org/10.1016/j.array.2026.100791
12. Benitez VH, Pacheco J, Cuamea-Cruz G. Lightweight deep learning for sEMG-based finger position classification and embedded system deployment. *IEEE Access*. 2025;13:38181-38194. https://doi.org/10.1109/ACCESS.2025.3545827
13. Simão M, Neto P, Gibaru O. EMG-based online classification of gestures with recurrent neural networks. *Pattern Recognit Lett*. 2019;128:45-51. https://doi.org/10.1016/j.patrec.2019.07.021
14. Hilton ML. Wavelet and wavelet packet compression of electrocardiograms. *IEEE Trans Biomed Eng*. 1997;44(5):394-402. https://doi.org/10.1109/10.568915
15. Pooyan M, Taheri A, Moazami-Goudarzi M, Saboori I. Wavelet compression of ECG signals using SPIHT algorithm. *Int J Med Health Sci*. 2007;1(2):85-88. https://doi.org/10.5281/zenodo.1072022
16. Dasan E, Gnanaraj R. Joint ECG–EMG–EEG signal compression and reconstruction with incremental multimodal autoencoder approach. *Circuits Syst Signal Process*. 2022;41(11):6152-6181. https://doi.org/10.1007/s00034-022-02071-x
17. Du X, Liang K, Lv Y, Qiu S. Fast reconstruction of EEG signal compression sensing based on deep learning. *Sci Rep*. 2024;14:5087. https://doi.org/10.1038/s41598-024-55334-9
18. Rhif M, Ben Abbes A, Farah IR, Martínez B, Sang Y. Wavelet transform application for/in non-stationary time-series analysis: a review. *Appl Sci*. 2019;9(7):1345. https://doi.org/10.3390/app9071345
19. Phinyomark A, Limsakul C, Phukpattaranont P. Application of wavelet analysis in EMG feature extraction for pattern classification. *Meas Sci Rev*. 2011;11(2):45-52. https://doi.org/10.2478/v10048-011-0009-y
20. Sitole SP, Sup FC. Continuous prediction of human joint mechanics using EMG signals: a review of model-based and model-free approaches. *IEEE Trans Med Robot Bionics*. 2023;5(3):528-546. https://doi.org/10.1109/TMRB.2023.3292451
21. Ramchandran K, Vetterli M. Best wavelet packet bases in a rate-distortion sense. *IEEE Trans Image Process*. 1993;2(2):160-175. https://doi.org/10.1109/83.217221
22. Kaaniche M, Fraysse A, Pesquet-Popescu B, Pesquet JC. A convex programming bit allocation method for sparse sources. In: *2012 Picture Coding Symposium*. IEEE; 2012:277-280. https://doi.org/10.1109/PCS.2012.6213346

23. Golilarz NA, Dehzangi I, Rahimi K. Optimized adaptive based method for MR image denoising. In: *2024 IEEE 16th International Conference on Computational Intelligence and Communication Networks (CICN)*. IEEE; 2024:976-983. https://doi.org/10.1109/CICN63059.2024.10847356

24. Trabuco MH, Costa MVC, Nascimento FAO. S EMG signal compression based on domain transformation and spectral shape dynamic bit allocation. *Biomed Eng Online*. 2014;13:22. https://doi.org/10.1186/1475-925X-13-22

25. Subasi A, Subasi ME, Qaisar SM. EEG-based biometric authentication using wavelet packet decomposition and ensemble classifiers. In: Naik GR, editor. *Time-Frequency Analysis in Biomedical Engineering*. 1st ed. CRC Press; 2026. https://doi.org/10.1201/9781003611448-17

26. Erkoc ME. A deep learning based compressed sensing method for electrocardiogram signals. *Circuits Syst Signal Process*. Published online 2026. https://doi.org/10.1007/s00034-026-03506-5

27. Piyathilaka L, Sul J, Arachchige SNSD. Advances in EMG signal processing and pattern recognition: techniques, challenges, and emerging applications. *Electronics*. 2026;15(3):590. https://doi.org/10.3390/electronics15030590

28. Anwar A, Khalifa Y, Coyle JL, Sejdic E. Transformers in biosignal analysis: a review. *Inf Fusion*. 2025;114:102697. https://doi.org/10.1016/j.inffus.2024.102697

29. Shin J, Miah ASM, Kabir MH, Rahim MA, Al Shiam A. A methodological and structural review of hand gesture recognition across diverse data modalities. *IEEE Access*. 2024;12:142606-142639. https://doi.org/10.1109/ACCESS.2024.3456436

30. Coifman RR, Wickerhauser MV. Entropy-based algorithms for best basis selection. *IEEE Trans Inf Theory*. 1992;38(2):713-718. https://doi.org/10.1109/18.119732

31. Meyer FG, Averbuch A, Strömberg JO. Fast adaptive wavelet packet image compression. *IEEE Trans Image Process*. 2000;9(5):792-800. https://doi.org/10.1109/83.841526

32. Al-Fahoum AS, Al-Fraihat AA. Methods of EEG signal features extraction using linear analysis in frequency and time-frequency domains. *Int Sch Res Notices*. 2014;2014:730218. https://doi.org/10.1155/2014/730218

33. Ma J, Bao X, Qin F, et al. CNN-MSTINet: a lightweight hybrid network with multi-scale temporal interaction for sparse sEMG-based gesture recognition. *Meas Sci Technol*. 2026;37(7):076111. https://doi.org/10.1088/1361-6501/ae44bc

34. Fraysse A, Pesquet-Popescu B, Pesquet J. On the uniform quantization of a class of sparse sources. *IEEE Trans Inf Theory*. 2009;55(7):3243-3263. https://doi.org/10.1109/TIT.2009.2021329

35. Atzori M, Gijsberts A, Heynen S, et al. Building the NinaPro database: a resource for the biorobotics community. In: *2012 4th IEEE RAS & EMBS International Conference on Biomedical Robotics and Biomechatronics (BioRob)*. IEEE; 2012:1258-1265. https://doi.org/10.1109/BioRob.2012.6290287

36. Howard PG, Vitter JS. Analysis of arithmetic coding for data compression. *Inf Process Manag*. 1992;28(6):749-763. https://doi.org/10.1016/0306-4573(92)90066-9

37. Yan T, Liang S, Mu L, et al. Adaptive Myo-spatial correction for overcoming electrode shifts impact in sEMG-based gesture recognition. *Biomed Signal Process Control*. 2025;103:107356. https://doi.org/10.1016/j.bspc.2024.107356

38. Li X, Zhang X, Zhang L, Chen X, Zhou P. A transformer-based multi-task learning framework for myoelectric pattern recognition supporting muscle force estimation. *IEEE Trans Neural Syst Rehabil Eng*. 2023;31:3255-3264. https://doi.org/10.1109/TNSRE.2023.3298797

39. Ji R, Tan K, Wang X, et al. PatchOut: a novel patch-free approach based on a transformer-CNN hybrid framework for fine-grained land-cover classification on large-scale airborne hyperspectral images. *Int J Appl Earth Obs Geoinf*. 2025;138:104457. https://doi.org/10.1016/j.jag.2025.104457

40. Guo W, Fouda ME, Eltawil AM, Salama KN. Neural coding in spiking neural networks: a comparative study for robust neuromorphic systems. *Front Neurosci*. 2021;15:638474. https://doi.org/10.3389/fnins.2021.638474